ARTICLE IN PRESS

Communications Earth & Environment https://doi.org/10.1038/s43247-026-03604-x

Article in Press

Arctic sea ice decline, increasing successive sudden stratospheric warmings and cold northern hemisphere continents

Received: 7 October 2025

Accepted: 1 May 2026

Cite this article as: Rao, J., Garfinkel, C.I., Cohen, J. *et al.* Arctic sea ice decline, increasing successive sudden stratospheric warmings and cold northern hemisphere continents. *Commun Earth Environ* (2026). https://doi.org/10.1038/s43247-026-03604-x

Jian Rao, Chaim I. Garfinkel, Judah Cohen, Yue Wang, Xiaoqi Zhang, Rongcai Ren & Pengfei Zhang

We are providing an unedited version of this manuscript to give early access to its findings. Before final publication, the manuscript will undergo further editing. Please note there may be errors present which affect the content, and all legal disclaimers apply.

If this paper is publishing under a Transparent Peer Review model then Peer Review reports will publish with the final article.

ARTICLE IN PRESS

© The Author(s) 2026. **Open Access** This article is licensed under a Creative Commons Attribution-NonCommercial-NoDerivatives 4.0 International License, which permits any non-commercial use, sharing, distribution and reproduction in any medium or format, as long as you give appropriate credit to the original author(s) and the source, provide a link to the Creative Commons licence, and indicate if you modified the licensed material. You do not have permission under this licence to share adapted material derived from this article or parts of it. The images or other third party material in this article are included in the article's Creative Commons licence, unless indicated otherwise in a credit line to the material. If material is not included in the article's Creative Commons licence and your intended use is not permitted by statutory regulation or exceeds the permitted use, you will need to obtain permission directly from the copyright holder. To view a copy of this licence, visit http://creativecommons.org/licenses/by-nc-nd/4.0/.

ARTICLE IN PRESS

Arctic sea ice decline, increasing successive sudden stratospheric warmings and cold northern hemisphere continents

Jian Rao[1, *], Chaim I. Garfinkel[2], Judah Cohen[3, 4], Yue Wang[1], Xiaoqi Zhang[1], Rongcai Ren[5], and Pengfei Zhang[6]

[1]State Key Laboratory of Environment Characteristics and Effects for Near-space / Key Laboratory of Meteorological Disaster of Ministry of Education, Nanjing University of Information Science and Technology, Nanjing, Jiangsu 210044, China

[2]Fredy and Nadine Herrmann Institute of Earth Sciences, The Hebrew University of Jerusalem, Edmond J. Safra Campus, Givat Ram Jerusalem 91904, Israel

[3]Atmospheric and Environmental Research, Lexington, MA, USA

[4]Department of Civil and Environmental Engineering, Massachusetts Institute of Technology, Cambridge, MA, USA

[5]State Key Laboratory of Numerical Modeling for Atmospheric Sciences and Geophysical Fluid Dynamics (LASG), Institute of Atmospheric Physics, Chinese Academy of Sciences, Beijing, 100029, China

[6]Department of Meteorology and Atmospheric Science, Pennsylvania State University, University Park, PA, USA

Corresponding authors: Dr. Jian Rao, raojian@nuist.edu.cn

ARTICLE IN PRESS

ARTICLE IN PRESS

Abstract

The frequency of successive sudden stratospheric warming events has markedly increased since 2000s. Using multimodel experiments it is demonstrated that reduced sea ice leads to higher frequencies of successive warming events. The decline in Arctic sea ice corresponds to a reduction in the refractive index in the mid-to-high latitude stratosphere, changing the waveguide and enhancing poleward planetary wave propagation. Decomposition of the refractive index reveals variations in the meridional gradient of potential vorticity are the dominant factor. Under reduced sea ice conditions, increased successive sudden warmings still produce persistent downward influences on surface weather, resulting in broader cold temperature anomalies across Northern Hemisphere continents. Further analysis of multimodel experiments confirms a significant negative correlation between Arctic sea ice and sudden warming frequency, ruling out greenhouse gases alone as the cause of the observed trend. As the Arctic warming reshapes stratospheric variability, the cold anomalies over some spots may not diminish.

Key words: Arctic sea ice; Sudden Stratospheric Warming (SSW); Cold extremes

ARTICLE IN PRESS

ARTICLE IN PRESS

Introduction

Sea ice plays a crucial role in global climate change by regulating heat, momentum, and moisture exchanges between the atmosphere and polar ocean, as well as redistributing salinity within the ocean. In the Arctic, the maximum sea ice extent occurs from late February to early April, while rapid retreat during spring and summer leads to an annual minimum in September[1]. Arctic sea ice is rapidly declining in the context of global warming[2-4]. Sea ice models project that the Arctic will be nearly ice-free in summer by the middle of the 21st century[5]. The reduction of Arctic sea ice is linked to various atmospheric and oceanic processes and can be attributed to the combined effects of internal climate variability and anthropogenic forcing[6-8]. Previous studies have found that observed sea ice decline can be partially attributed to anthropogenic greenhouse gas emissions[6,9-11]. Atmospheric and oceanic variability, such as the North Atlantic Oscillation (NAO), the Atlantic Multi-decadal Oscillation (AMO) and Atlantic Meridional Overturning Circulation (AMOC), influence changes in Arctic sea ice[12-16].

Arctic sea ice decline not only affects local weather and climate, but also exerts remote hemispheric influences, contributing to midlatitude weather and climate variability and changes in extremes[17-20]. Arctic sea ice reduction amplifies near-surface warming in the Arctic lower troposphere and increases atmospheric moisture and cloud cover[21-23]. Arctic sea ice loss can trigger negative phases of the North Atlantic Oscillation (NAO) and Arctic Oscillation (AO), weaken meridional temperature gradients, increase blocking frequency, and intensify midlatitude extreme events[24-27]. Arctic sea ice decline also affects the stratospheric polar vortex by changing the wave activities and the environment where waves propagate. For example, when ice loss is concentrated in the Arctic North Atlantic sector (Barents-Kara, Greenland, and Labrador Seas), the winter polar vortex weakens as wave activities are enhanced. Conversely, ice loss in the Arctic North Pacific sector (Bering and Okhotsk Seas) leads to polar vortex strengthening[28]. Stratospheric signals associated with weakening or strengthening of the stratospheric polar vortex can propagate downward, inducing negative or positive phases of the Arctic Oscillation (AO) in the troposphere[19,29].

ARTICLE IN PRESS

Sudden stratospheric warming (SSW) events are the most spectacular stratospheric events, and are characterized by a rapid temperature rise in the polar stratosphere during winter and a marked weakening of the stratospheric polar vortex (SPV)[30,31]. SSW events were infrequent in the 1990s but have occurred more frequently since 2000[32]. The propagation and breaking of planetary waves play a key role in the onset and evolution of SSW, and most SSW events are associated with significant changes in planetary wave activity[33,34]. El Niño-Southern Oscillation (ENSO), the quasi-biennial oscillation (QBO), and sea surface temperature (SST) anomalies influence SSW events by modulating the upward propagation of planetary waves[35-38]. Arctic sea ice also modulates planetary wave propagation, thereby influencing SSW events[19,39]. The Barents-Kara Sea (BKS) has been identified as a key source region for the stationary Rossby wave response, modulating the upward propagation of planetary waves[19,40]. The stratosphere-troposphere interaction may provide a memory in the lagged sea ice impact: Positive (negative) sea ice concentration anomalies in November are associated with a strengthened (weakened) stratospheric polar vortex and these anomalies propagate downward leading to the positive (negative) NAO-like pattern in the late December to early January[41]. As a result, positive (negative) Barents-Kara sea ice concentration anomalies in autumn are associated with a positive (negative) NAO pattern with lags of up to 3 months[41]. Observational and modelling studies show that upward wave propagation during weak polar vortex events in heavy-ice years is dominated by the wavenumber 1 component, while weak polar vortex event in light-ice years is dominated by the wavenumber 2[42].

A recent modeling study finds that multiple SSWs can occur in one winter, and that the surface impacts from multi-SSW winters are more evident than single SSW winters[43]. In the 2022/23 winter, two SSWs occurred successively[44], one in January and one in February (Figure 1a), accompanied by Northern Hemisphere continental cold events. Cold air frequently broke out southward in East and Southeast Asia in January, and the cold wave reached even further south later. In the western hemisphere, cold waves occurred in Northeast North America, and more snowstorms hit Southern California (Figure 1e). In the 2023/24 winter, three SSWs occurred one after the other in January, February, and March, respectively, although due to the close proximity

ARTICLE IN PRESS

in time, the second and third SSWs were considered as one event[45] (Figure 1b). Three SSWs appearing in one winter was observed for the first time since 1979 and likely even earlier[46]. More and broader cold waves hit the NH continents in this winter. For example, cold air outbreaks hit Mongolia, North India, Bangladesh, Northern Europe, United Kingdom, and the United States in January 2024. Extreme cold outbreaks have not been limited to these two recent winters and a recent study found no statistically significant reduction in cold extremes over large parts of the Northern Hemisphere during the period of Arctic amplification[47]. Multiple SSWs occurred in winter 2025/26 also accompanied by cold air outbreaks across Eurasia and North America.

It has been observed that SSW winters have become more frequent, including more frequent multi-SSW winters[44,46,48]. Concurrently, the Arctic Ocean SIC was anomalously low in the autumn of 2022 and 2023[42,43]. However, it is still unknown if this is just sampling variability, or if there is a linkage between the sea ice concentration (SIC) decrease and the increase of SSWs and multi-SSW winters.

Considering that the limited number of observed multi-SSW winters cannot causally demonstrate a SIC –SSW relationship, sensitivity experiments and ample outputs from models participating in Coupled Model intercomparison Project Phase six (CMIP6) can constitute a large ensemble suited to help explore their link. The present study aims to answer the following two questions: (1) Is there any statistical and dynamical relationship between Arctic SIC decline and increased SSWs? (2) What consequences are observed and projected if both are linked?

ARTICLE IN PRESS

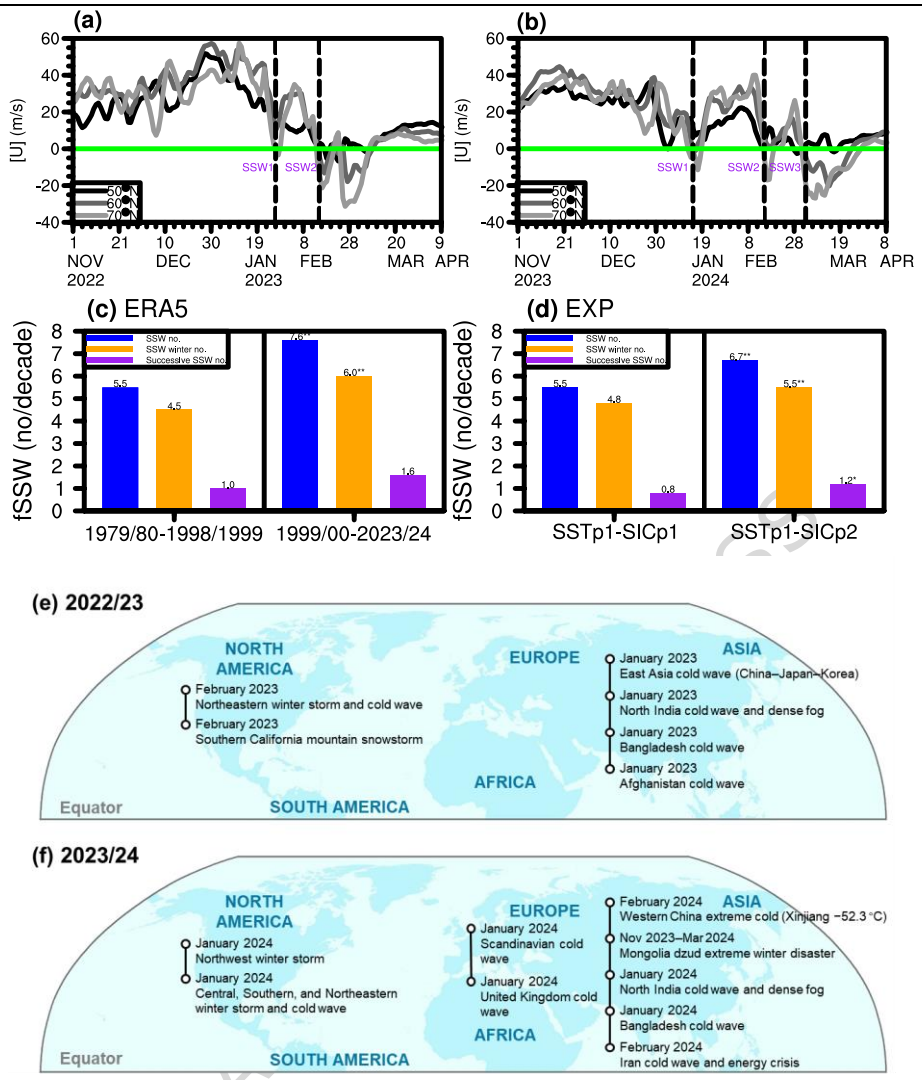

Figure 1. Winter when successive Sudden Stratospheric Warmings (SSWs) occur (multi-SSW winter).

(a, b) Observed successive SSWs in the 2022/23 and 2023/24 winters, respectively. Evolution of the zonal mean zonal winds (units: m/s) at 60°N and 10 hPa (U60) is displayed (c) Statistics of successive U60 SSWs in two periods: 1979/80-1998/99 versus 1999/00-2023/24 based on the ERA5 reanalysis (units: no. per decade). (d) The statistics of successive SSWs in two experiments using the CESM2-WACCM model. SSTp1-SICp1 is forced by observed sea surface temperature (SST) and Arctic sea ice concentration (SIC) during 1979/80. SSTp1-SICp2 is similar to the SSTp1-SICp1 run except that the Arctic SIC during 1999/00-2023/24 is used. The single and double asterisks in c, d mark the difference between two samples at the 90% and 85% confidence level, respectively. Blue bars show the total SSWs, orange bars show the total winters with at least one SSW, and purple bars show the total winters with at least two SSWs. All three quantities are shown as numbers per decade. (e, f) Northern Hemisphere land cold waves in two multi-SSW years.

ARTICLE IN PRESS

In this work, we examine the relationship between Arctic SIC and SSWs, particularly successive SSWs, using reanalysis data, observations, and sensitivity experiments. A series of experiments from a high-skill CMIP6 model are conducted to examine the relationship between Arctic SIC and SSWs and the possible mechanism. Finally, multi-model outputs are analyzed to further validate the association between Arctic SIC and (successive) SSW frequency.

Results

Successive SSWs and continental coldness: reanalysis and bespoke simulations

The co-occurrence of successive SSWs and active cold air outbreaks (Figure 1) suggests that SSWs in winter can lead to cold air outbreaks over land. However, we still do not know what may have caused the occurrence of successive SSWs. The SSW frequency and the multi-SSW winter frequency is compared during two periods: 1979/80-1998/99 versus 1999/00-2023/24 (Figure 1c). It is revealed that the SSW frequency increased in recent two decades from 5.5 to 7.6 per 10 years, winters with at least one SSW increased from 4.5 to 6.0 per 10 years, and multi-SSW winters increase from 1.0 to 1.6 per 10 years. To source the possible driving force of the SSW increase, two experiments are performed using CESM2-WACCM (Figure 1d). When the SIC is fixed at the post-2000 level, the SSW frequency (5.5 vs 6.7 per 10 years), SSW winters (4.8 vs 5.5 per 10 years), and multi-SSW winters increase relative to the experiment with SIC fixed at the 1979-1999 level (All those changes are significant at the 90% confidence level based on a bootstrap test). It should be emphasized that multi-SSW winters increase from 0.8 to 1.2 per 10 years, which is primarily caused by the Arctic SIC decline, since the forcing is identical for the two experiments except that the SIC is different.

To give an explanation of the SSW frequency change, Figure 2 compares the atmospheric dynamics during the two periods. When the SIC decreases over the Arctic marginal seas (Figure 2c-d), the refractive index (n^2) is changed in mid-to-high latitudes (Figure 2f). During 1979-1999 when the Arctic SIC was still broad (Figure 2a), the refractive index was positive in most of the extratropics from the troposphere to stratosphere (Figure 2e). A maximum positive refractive index

band extends from the subtropical upper stratosphere to the extratropical lower stratosphere (see the purple box in Figure 2e). Another maximum refractive index band is situated over the polar lower stratosphere. Planetary waves tend to travel and inflect toward high refractive index regions and trapped where negative refractive index develops. Along with the high n^2 value, two wave guides are observed; one to the lower stratosphere over the Arctic, and the other to the subtropical upper stratosphere (Figure 2g).

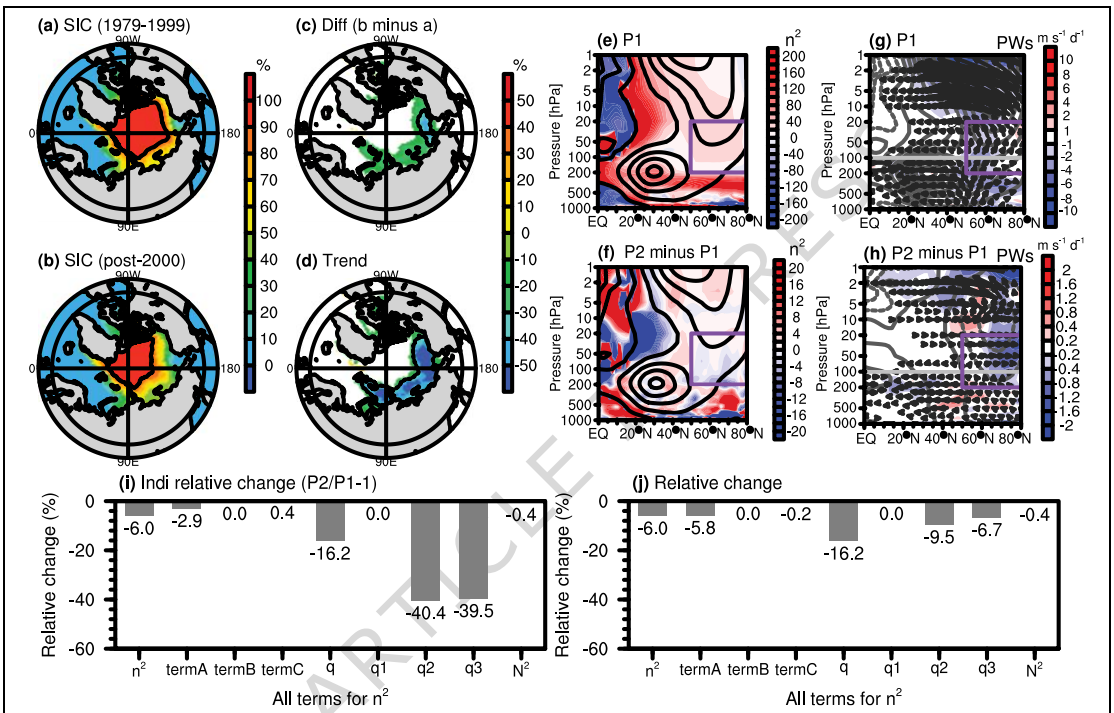

Figure 2. Change in Arctic SIC and atmospheric dynamics.
(a, b) Multiyear mean Arctic SIC (units: %) in the Northern Hemisphere autumn for 1979-1999 and post-2000 periods (P1 and P2), respectively. (c) Autumn SIC difference between P2 and P1 (units: %). (d) The trend of the autumn Arctic SIC since 1979 (normalized to %/40 years). (e) Winter mean (December–February) atmospheric refractive index during P1. (f) Changes in the winter mean refractive index from P1 to P2. The contours in e and f show the corresponding zonal mean zonal winds (units: m/s) during P1 and P2, respectively. The contour interval is 10 m/s with easterlies in dashed lines, westerlies in solid lines, and zero winds in thickened lines. (g) Winter mean Eliasson-Palm (EP) flux (vectors), EP flux divergence (units: m/s/d, shadings), and zonal mean zonal winds (units: m/s, contours). (h) Changes in the winter mean EP flux, EP flux divergence, and zonal mean zonal winds from P1 to P2. The purple box in e-h shows the key region where the wave refractive index has decreased and the poleward wave propagation enhanced. (i) Relative changes in the wave refractive index (n^2) and each term for the

ARTICLE IN PRESS

purple box in e-h. See the text for each term description. (j) As in (i) but the change in term A-C is relative to their total (n^2), and the change in q1-3 is relative to their total (q).

In the last two decades, the refractive index in mid-to-high latitude stratosphere (200–20 hPa) has decreased when the Arctic SIC also declined (Figure 2f). Namely, the bottom of the maximum n^2 band extending from the subtropical upper stratosphere has lessened, which has led to a decrease of equatorward propagating waves as marked by the positive difference (poleward directed arrows) of the meridional component of the EP flux (F_φ, see Methods) in the purple box (Figure 2h). As a consequence, more planetary waves are dissipated in the Arctic stratosphere, so the E-P flux convergence in the Arctic stratosphere has increased in the past two decades. The increased wave forcing in the lower-to-mid stratosphere over the Arctic is also reported in Zhang et al.[39], where the response to sea ice loss in large ensemble simulations is examined.

The changes of n^2 can be decomposed into three terms, marked as A – C (Figure 2i, j). Term A is proportional to the zonal-mean quasi-geostrophic potential vorticity meridional derivative ($\bar{q}_\varphi$) divided by mean zonal winds ($\bar{u}$). Term B is a constant that only depends on the latitude and wavenumber, which does not vary with the time. Term C depends on the change of the Brunt-Väisälä frequency. The refractive index in the Arctic stratosphere decreases by 6%, which was mainly contributed by the term A. Term A decreases by 2.9% relative to its climatology and contributed -5.8% of the total decrease in n^2 (-6%). Namely, nearly all of the refractive index decrease (-6%) is caused by the decline in term A (-5.8%), which equals $\bar{q}_\varphi$ divided by $a\bar{u}$ (a is the radius of the Earth). Therefore, to understand the reasons for the decrease in term A, the changes in q and $a\bar{u}$ should also be examined. q decreases by -16.2% and while $a\bar{u}$ also decreases (Figure 2h), the net total effect is that the decrease of q (-16.2%) overwhelms the change of $\bar{u}$ and leads to -5.8% changes in n^2. The change in $\bar{q}_\varphi$ is caused by q2 and q3 (nearly proportional to $\bar{u}_{\varphi\varphi}$ and $\bar{u}_{zz}$, respectively, see Methods) decreases, explaining -9.5% and -6.7% of the total -16.2% change in q, respectively. Although term C is also decreasing, it only explains -0.2% in the total -6% n^2 change. This decrease in term C is consistent with the decrease in Brunt-Väisälä frequency.

Evidence from multiple CMIP6 experiments in an individual model

Limited samples from reanalysis are not enough for the attribution of the SSW frequency change. Outputs from the NCAR model CESM2-WACCM are long enough to provide a large number of multi-SSW samples and SIC diversity. We choose the piControl experiment as the reference state when the Arctic SIC is the most extensive. Different experiments with available SIC outputs and their ensembles are gathered and shown in Figure 3. Compared with piControl (~58% coverage), Arctic SIC decreases in all remaining experiments (Figure 3a-j). The Arctic Ocean is nearly open without sea ice coverage in abrupt-4xCO2, while the SIC still extends over ~56% in historical runs (Figure 3k, l), with a decrease of ~2% (Figure 3b). Previous studies have reported that sea ice decline inevitably increases planetary wave activities, which disturbs the stratospheric polar vortex. Next, we will examine whether SIC decline has a relationship with SSW using the abundant output data.

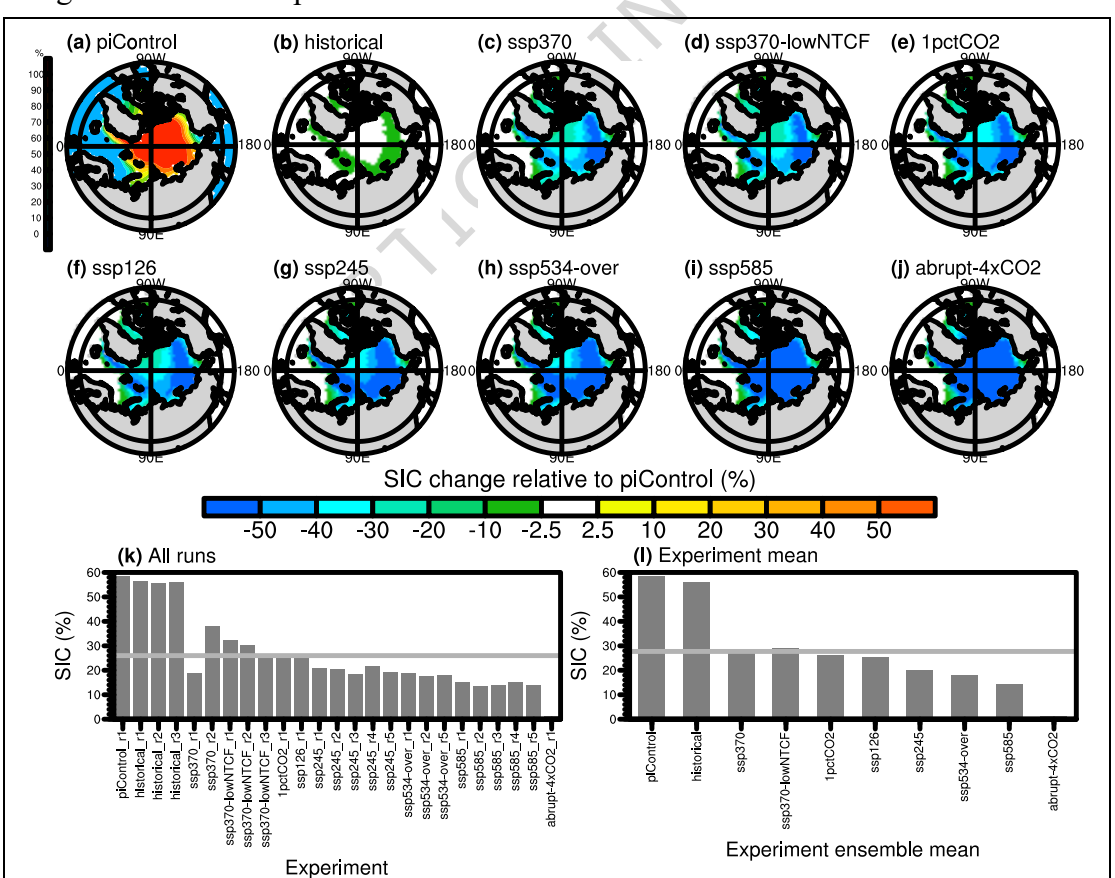

Figure 3. Autumn Arctic SIC change in different experiments relative to piControl.

ARTICLE IN PRESS

(a) Autumn Arctic SIC (units: %) in the piControl run. (b-j) Differences in autumn Arctic SIC (units: %) for different experiments relative to the piControl run. The multi-member mean is shown if the experiment has multiple members (historical, ssp245, ssp370, ssp370-lowNTCF, ssp534-over, and ssp585). Full fields are shown in Supplementary Figure 1. (k) Simulated mean autumn Arctic SIC (units: %) over the Arctic Ocean for all experiments. Multiple members are shown if applicable. (l) As in k but for the multi-member mean for the experiments with different members.

Figure 4 gives the statistics of SSW frequency and multi-SSW winter frequency for all CESM2-WACCM experiments in which daily u-winds and monthly SIC outputs are available. Figure 4b, c shows the relationship between the SSW frequency vs the SIC and the multi-SSW winter frequency vs the SIC. The SSW frequency is negatively correlated with the Arctic SIC, whereby lower SIC is associated with more frequent SSW. The SSW frequency in piControl and three historical runs with high SIC is relatively less than the future warming scenarios with low SIC (Supplementary Figure 2). The correlation decreases (amplitude increases) to -0.79 (significant at the 99% confidence level) if only the experiment ensemble mean is considered, while it is -0.35 for all members of all experiments (Figure 4b vs Supplementary Figure 2b). The multi-SSW winter is also negatively correlated with the mean SIC if only the experiment ensemble mean is considered, although the correlation (-0.43) is less significant possibly due to a limited sample size (Figure 4c).

ARTICLE IN PRESS

ARTICLE IN PRESS

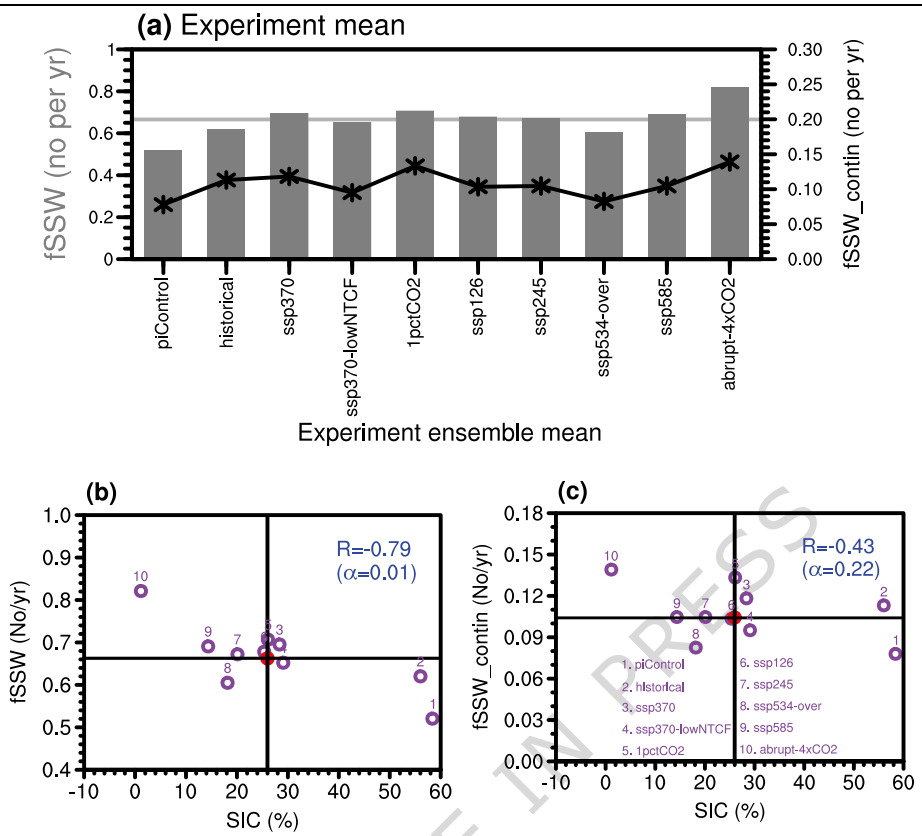

Figure 4. Statistics of the SSW frequency and multi-SSW winter frequency in a series of experiments.
(a) Bar plot of SSW frequency (fSSW; units: no/yr) in a series of experiments (multi-member mean if applicable) with the multi-SSW winter frequency (fSSW_contin; units: no/yr) shown in asterisk and curve. (b) Scatter plot of the Arctic SIC (units: %) versus the SSW frequency. The correlation between the SIC and the SSW frequency and its significance are shown in the top right corner. (c) As in b but for the scatter plot of the SIC versus the multi-SSW winter frequency. Individual ensemble members are shown in Supplementary Figure 2.

The evolution of the u-winds and their anomalies in the stratosphere during SSWs is similar among the different experiments (Figure 5a, b). Namely, the general stratospheric features of SSWs are similar for all experiments[49]. However, the persistence of negative u-wind anomalies and downward impacts of SSWs are diverse among those experiments, and experiments with lower SIC tend to have a strengthened near-surface response (Figure 5c-l). In piControl, historical, and ssp126 runs, the surface impact of SSWs rapidly follows the SSW onset (Figure 5c, d, h). However, the near surface impact is not continuous in those experiments with high Arctic SIC. In 1ptCO2, abrupt-4xCO2, ssp245, ssp370, and ssp585, the near surface anomalies are larger, more continuous,

ARTICLE IN PRESS

and more persistent.

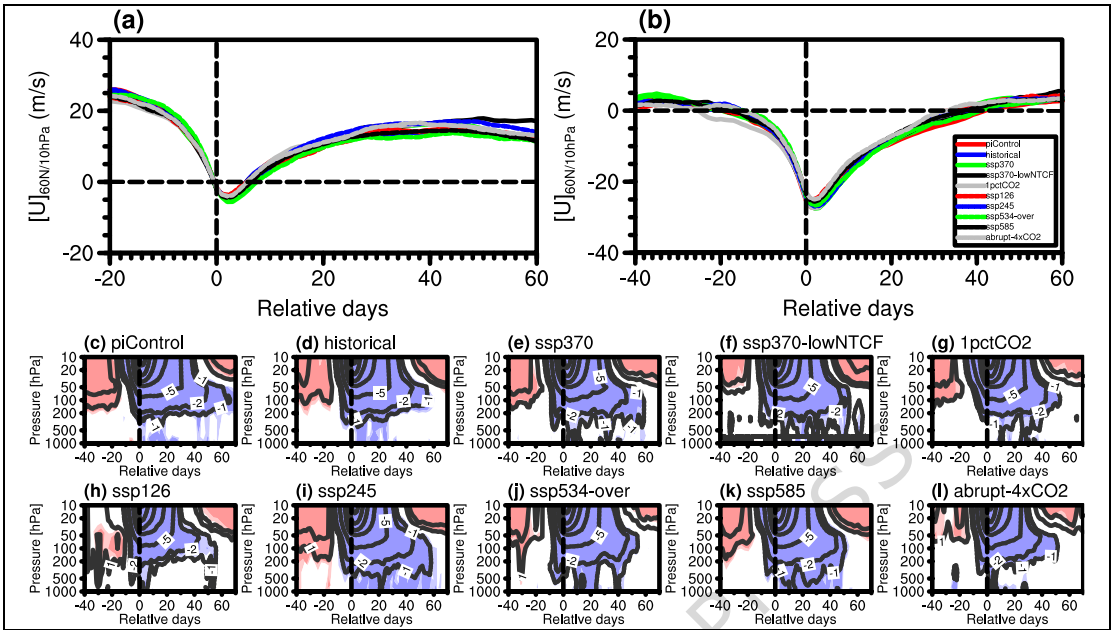

Figure 5. Composite evolution of SSWs in different experiments.
(a) Composite evolution of zonal mean u-winds (units: m/s) at 60°N and 10 hPa in different experiments (multi-member mean). (b) As in a, but for zonal mean u-wind anomalies (units: m/s). Individual ensemble members are shown in Supplementary Figure 3. (c-l) Height-time evolutions of zonal mean u-wind anomalies at 60°N from 1000–10 hPa for different experiments (contours, units: m/s). The light and dark shading show the composite u-wind anomalies at the 90% and 95% confidence levels, respectively (red for positive and blue for negative).

This strengthened downward impact of SSWs in the presence of low SIC might lead to cold air outbreaks, and could contribute to the frequent cold outbreaks in recent years as the Arctic SIC is declining. For example, sensitivity experiments forced by decreased Arctic Ocean SIC produce broad cold anomalies over the Northern Hemisphere continents[39], although the midlatitude cold extremes are observed and simulated to decrease over recent decades[50]. We explore this possibility in Figure 6, which shows the composite surface air temperature (tas) anomalies averaged from days 10-55 with respect to the corresponding climatology. Consistent with the downward impact of the u-wind anomalies in Figure 5, the cold anomalies are primarily confined to a narrow area of northern Eurasia in piControl run (Figure 6a), but gradually broaden in other experiments with SIC decline. In the historical run, scattered cold anomalies begin to appear in US (Figure 6b), which is consistent with observations that cold air outbreaks appear in US following SSW onset (Figure 1).

ARTICLE IN PRESS

In all experiments examined here (1pctCO2, abrupt-4xCO2, ssp370-lowNTCF, and ssp534-over are removed due to their small SSW sizes, see Supplementary Tables 1 and 2) with less SIC than in historical and piControl runs, the SSW impact is not weakened especially over US (Figure 6c-f). Specifically, the cold anomalies over northern Eurasia and the US are larger in ScenarioMIP experiments with SIC decline than in historical and piControl runs. The cold anomalies over the US spread farther south, which might imply that the anomalous cold air outbreaks can still affect the midlatitudes in a world with less Arctic SIC when more SSWs and successive SSWs happen. Over the coming decades there is strong evidence that cold anomalies will still occur alongside more frequent SSWs under the background of the Arctic SIC decline.

ARTICLE IN PRESS

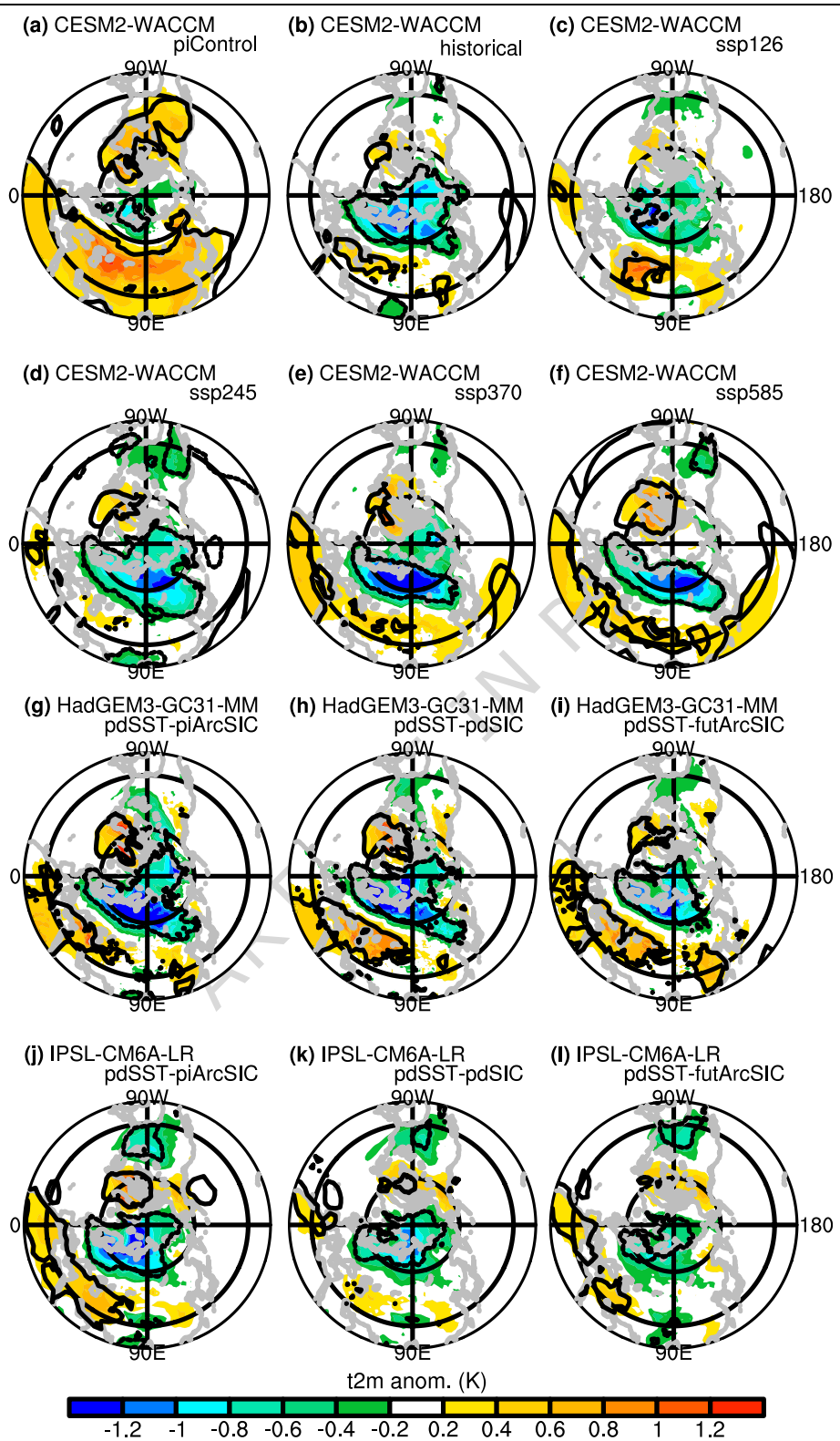

Figure 6. Surface atmospheric temperature anomalies following SSW onset. (a-f) Composite surface atmospheric temperature (tas) anomalies during days 10-55 after the SSW onset for different CESM2-WACCM experiments (shadings, units:

K). The anomalies for each experiment are the deviations from its own climatology. (g-i) As in a-f but for the PAMIP experiments from HadGEM3-GC31-MM. Three PAMIP experiments are examined, including pdSST-piArcSIC, pdSST-pdSIC, and pdSST-futArcSIC. (j-l) As in g-i but for PAMIP experiments from IPSL-CM6A-LR. The contours show the composite tas anomalies at the 95% confidence level.

To further minimize the possible interference of other forcings with the SSW downward impact in a world with less Arctic SIC, the Polar Amplification Model Intercomparison Project (PAMIP) experiments are helpful. Three PAMIP experiments are analyzed, and they are present-day SST present-day SIC run (pdSST-pdSIC), present-day SST future SIC run (pdSST-futArcSIC), and present-day SST preindustrial SIC run (pdSST-piArcSIC). Out of the four PAMIP models that have daily u-winds available, only two can reasonably simulate the SSW frequency (Figure 7). AWI-CM-1-MR simulates too many SSWs, and CanESM5 simulates too few SSWs.

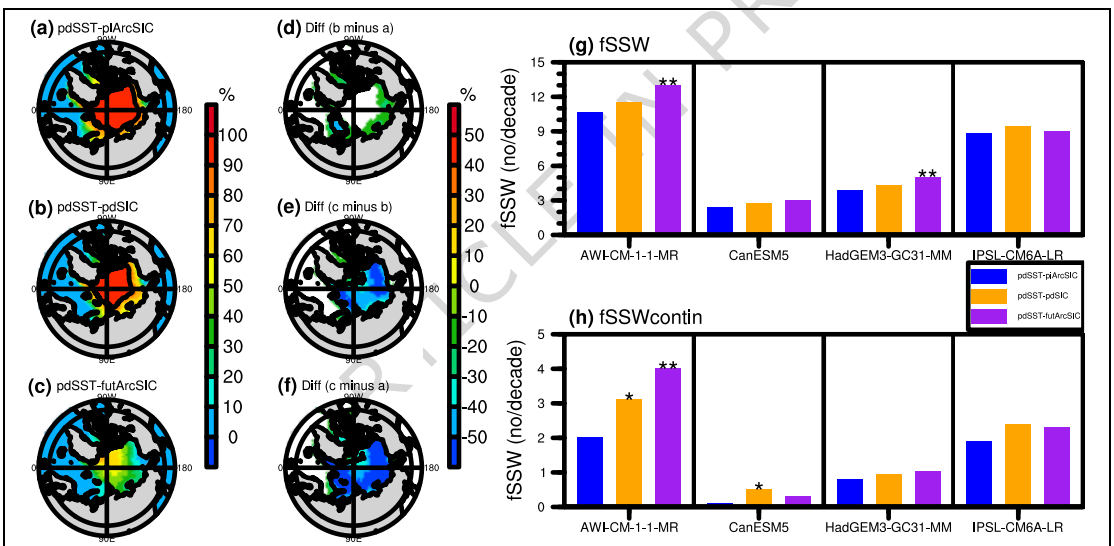

Figure 7. SIC forcings and SSW responses in PAMIP experiments.
(a-c) Mean Arctic SIC (units: %) forcings in the Northern Hemisphere autumn for three sensitivity experiments (pdSST-piArcSIC, pdSST-pdSIC, and pdSST-futArcSIC). (d-f) Difference in the Arctic SIC between any two of the three sensitivity experiments. (g) Statistics of SSWs in the three sensitivity experiments from four PAMIP models with all of the three runs available. (h) As in g but for the successive SSWs.

HadGEM3-GC31-MM and IPSL-CM6A-LR also have decent stratospheric variability, and they simulate better SSW frequency[49] and/or increased successive SSWs. In PAMIP, these two models show that the cold anomalies across northern Eurasia and North America following SSWs in pdSST-futArcSIC do not strengthen but spread farther southward in North America when

ARTICLE IN PRESS

compared with those in pdSST-pdSIC and pdSST-piArcSIC (Figure 6g-l). In both PAMIP models, the cold anomaly coverage in northern Eurasia is nearly unchanged from pdSST-piArcSIC to pdSST-pdSIC and then to pdSST-futArcSIC. However, the cold anomalies over South Canada and the United States move farther southward gradually.

Observational evidence has shown that the increased SSWs in recent decades might be related to the decline of the refractive index from the tropical upper stratosphere to the midlatitude lower stratosphere. Similar changes are also found in the CMIP6 experiments for CESM2-WACCM: Relative to piControl, all the remaining experiments show a n^2 decline in the mid-to-high latitude stratosphere (Figure 8a-j), which are usually consistent with the decrease of equatorward propagating planetary waves and increase of poleward propagating waves in the Arctic stratosphere. The changes in n^2 are consistent with the SSW frequency among experiments. For PAMIP runs, four models simulate a decline in the refractive index in pdSST-pdSIC and pdSST-futArcSIC relative to pdSST-piArcSIC (Supplementary Figures S5 and S6), consistent with the increased SSW and successive-SSW frequency (Figure 7g, h).

The key chain to explain the SIC – SSW relationship is to examine whether the Arctic SIC affects n^2. The scatter plot of the Arctic SIC versus n^2 is shown in Figure 8k-p among experiments for CESM2-WACCM. There is a robust and significant correlation of SIC with n^2, with an inter-experiment correlation of 0.90 (Figure 8k). This effect, coupled with the reanalysis results, might demonstrate that SIC decline can lead to n^2 decline, which finally results in a decrease of equatorward propagating planetary waves. The impact of SIC on n^2 is comparably contributed by changes in term A and term C (Figure 8l, m), since the inter-experiment correlation is similar in Figure 8k, l. This is consistent with the observed changes in n^2 that is also dominated by term A. The changes in term A are predominantly contributed by $q2$, which has a correlation of 0.91 with the SIC (Figure 8n). However. the correlation sign is reversed for $q3$ (Figure 8o), which implies that changes in $q3$ cancel the effect of changes in $q2$, and the total effect of $q2$ and $q3$ lead to a correlation of 0.85 between SIC and term A (or q) assuming $\bar{u}$ is unchanged (this assumption is somewhat reasonable, since the u-winds in Figure 8a-j are very similar). The scatter plot between

ARTICLE IN PRESS

SIC versus N^2 and that between SIC versus term C are nearly identical (Figure 8m, p; see the methods for explanation).

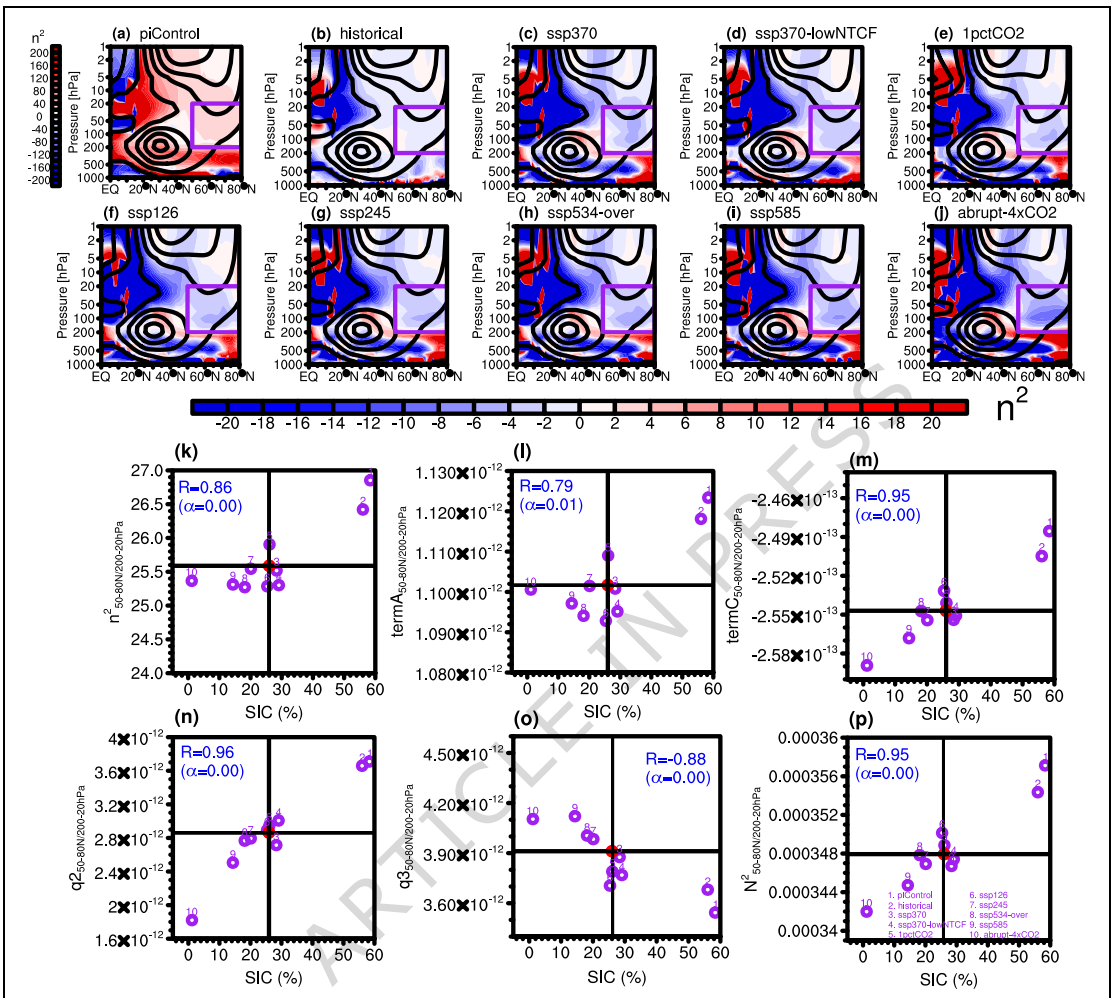

Figure 8. Variations of the atmospheric refractive index with the SIC.
(a) Distribution of the atmospheric refractive index (n^2) in the CESM2-WACCM piControl experiment. (b-j) Differences in the refractive index between a series of experiments and the piControl run. The contours show zonal mean zonal winds (units: m/s, interval: 10). (k) Scatter plot of the SIC versus the refractive index. (l, m) Scatter plot of decomposition of the refractive index into different terms (term B only depends on the geographic position, not shown) versus the SIC. (n, o) Scatter plot of decomposition of the term A into different sub-terms (subterm q1 only depends on the wavenumber, not shown). (p) Scatter plot of the SIC versus the buoyancy frequency (N^2), consistent with m (see the text). The n^2 index and all its terms and sub-terms are averaged over the subpolar region (50-80 N, 200-20 hPa). Individual ensemble members for k-p are shown in Supplementary Figure 4.

Evidence from multiple models

ARTICLE IN PRESS

The analysis from multiple experiments provided strong evidence that future declines in SIC will lead to more SSWs with a stronger surface impact in CESM2-WACCM. However, there are two limitations to this result: i) it is difficult to distinguish the importance of the Arctic SIC decline vs. the influence from increasing greenhouse gases, and the changes in SSW frequency (or successive SSWs) could instead be mainly associated with increasing greenhouse gases; ii) it is based on a single model, and other models might show different sensitivities. As a complement, we now analyze the historical runs of 34 CMIP6 models with available daily u-winds and monthly SIC, contrasted with only two PAMIP models. The simulated historical SIC mean state and the SSW frequency are shown in Figure 9. It is revealed the autumn SIC in the Arctic Ocean varies with the model for historical runs (Figure 9a), which provide diverse Arctic SIC states and therefore can be used to build the possible relationship between SIC and SSW frequency (or/and successive SSWs).

ARTICLE IN PRESS

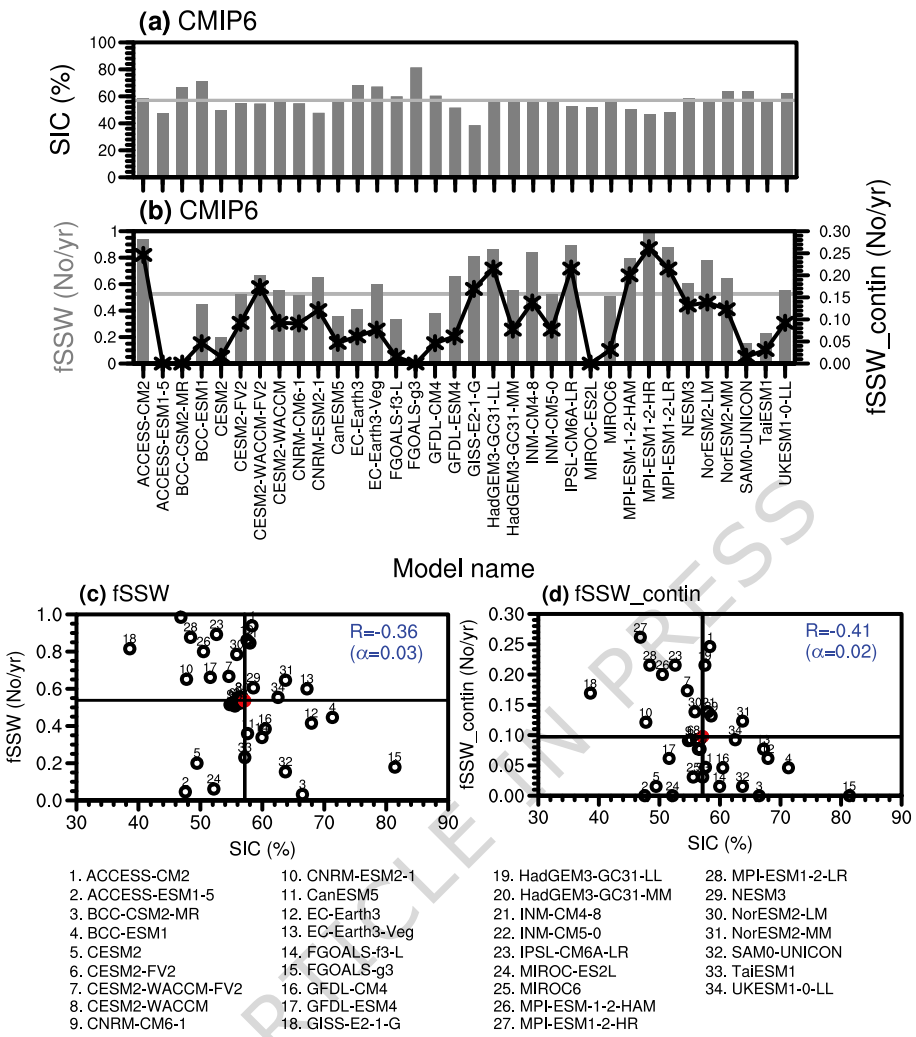

Figure 9. Relationship between Arctic SIC and multi-SSW winter frequency in CMIP6.

(a) Bar plot of autumn mean SIC (units: %) in the Arctic Ocean for CMIP6 models. The first ensemble member from historical runs (1950-2014) is used for each model. (b) The SSW frequency (units: no/yr) and the multi-SSW frequency (units: no/yr) in CMIP6 models. (c) Scatter plot of the Arctic SIC state versus the SSW frequency with the intermodel correlation and its significance level printed on the top right. (d) As in c but for scatter plot of the Arctic SIC state versus the multi-SSW winter frequency.

The SIC multimodel ensemble mean is around 57% in the Arctic Ocean (Figure 9a). The SSW frequency in the multimodel ensemble mean is 0.5 per year, while different models show various SSW frequency (Figure 9b). Models with high SIC usually produces less SSWs and less multi-SSW winters (e.g., BCC-CSM2-MR and FGOALS-g3). Models with low SIC, on the other hand, produce more SSWs. These results are consistent with PAMIP experiments: the pdSST-pdSIC

ARTICLE IN PRESS

and/or pdSST-futArcSIC run produces higher (successive) SSW frequencies than the pdSST-piArcSIC run (Figure 7). The scatter plot of the SIC versus the SSW frequency among CMIP6 models is shown in Figure 9c, which provides evidence that the mean SIC state influences the SSW frequency. The correlation between SIC and SSW frequency is -0.36 at the 97% confidence level. Although correlation magnitude among models is smaller than that among experiments for CESM2-WACCM (-0.79, Figure 4b), the significance level is still high due to a large sample size of models.

Similarly, the SIC decline not only influences the SSW frequency, but also exerts a potential impact on the multi-SSW winter frequency (Figure 9d). The correlation between the SIC and successive SSW frequency is -0.41 among models, with a comparable magnitude to that among experiments for CESM2-WACCM (-0.43, Figure 4c). The relationship between the SIC and successive SSWs among models is significant at the 98% confidence level, higher than that for the CESM2-WACCM experiments (Figure 4c). The CMIP6 multimodel results provide more robust evidence that the recent increased successive SSWs are very likely forced by the Arctic SIC decline. All those results suggest that anomalous cold air outbreaks in the future might not weaken in the coming decades, and the stratospheric variability associated with a less Arctic SIC state is still an effective indicator for a high possibility of anomalous cold air outbreaks especially over North American midlatitudes.

ARTICLE IN PRESS

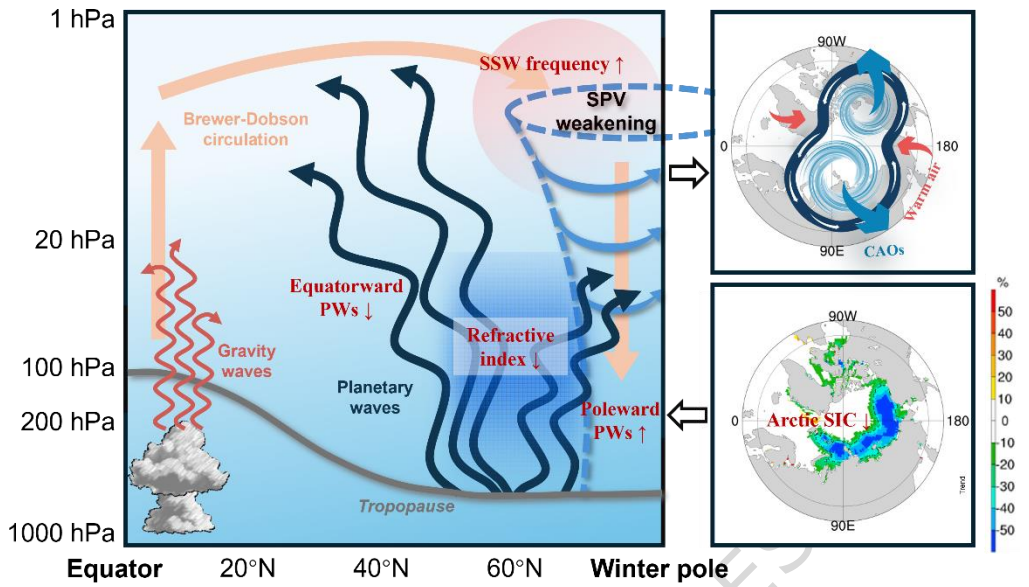

Figure 10. Schematic chart for Arctic SIC decline, SSWs, and cold air outbreak. As the Arctic SIC declines, the Arctic warms and the refractive index decreases, which leads to enhanced poleward propagation of planetary waves. As a consequence, the stratospheric polar vortex is more easily disturbed in a world with less Arctic SIC, explaining the increased successive SSWs. The displaced, distorted or split vortex carries cold air southward. The anomalous coldness covered regions are projected to shift farther southward especially in North America.

Discussion

Recent winters (e.g., 2022/23, 2023/24, 2025/26) have experienced an increased frequency of SSW events, with more than one SSWs observed each winter. These events were consistently accompanied by anomalous cold air outbreaks across North America and Eurasia. This research investigates the relationship between the Arctic SIC decline and increased successive SSWs, and implies that these successive SSWs increased the likelihood for cold air outbreaks over Northern Hemisphere continents in recent winters.

The SSW frequency in the past 25 years has increased compared to the late 20th century, and the frequency of multi-SSW winters has also increased from once every 10 years to once every six years. The changes in the SSW and multi-SSW winter frequencies are consistent with the Arctic

ARTICLE IN PRESS

SIC decline. To validate their relationship, a sensitivity experiment forced by post-2000 Arctic SIC using the CESM2-WACCM model is compared with the control experiment forced by the 1979-1999 climate SIC. The SSW frequency and the multi-SSW winter frequency in the sensitivity experiment is higher than in the control experiment, further verified by PAMIP experiments (pdSST-piArcSIC vs pdSST-pdSIC vs pdSST-futArcSIC). The SIC decline is possibly the primary driver behind the increased SSW frequency.

The mechanism whereby the SIC decline influences the SSW frequency and the multi-SSW winter is analyzed (Figure 10). Arctic SIC decline leads to enhanced poleward wave activity over the mid-to-high latitude stratosphere by changing the environment where waves propagate, which is confirmed by the decrease of the refractive index (n^2) changes. Namely, Arctic SIC loss reduces the refractive index in the mid-to-high latitude stratosphere, which weakens a wave guide that normally directs planetary waves equatorward. A decomposition of n^2 changes further reveals that the term A (the quasi-geostrophic potential vorticity meridional gradient) contributes to most of those changes, and term C (a term determined by atmospheric static stability) shows a minor role.

An assessment of the CESM2-WACCM experiments further confirms that the changes in n^2 is predominantly caused by changes in potential vorticity meridional gradients. With the SIC decline, the potential vorticity meridional gradient weakens, which finally exert a direct influence on n^2. Although the decline of atmospheric static stability is also identified, the term incorporating it (term C) plays a minor role.

In a world with less Arctic SIC, SSWs and multi-SSW winters are simulated to become more frequent, and the downward impact of SSWs on surface weather might not weaken. This still leads to broad and cold temperature anomalies over northern continents, especially across North America and Eurasia, explaining the observed anomalous cold outbreaks in recent years[47].

To minimize the possible interference of greenhouse gas within the SIC influence, and to show robustness in other models, analysis of PAMIP experiments with multimodel historical runs from CMIP6 is provided. At least two PAMIP models show that the SSW and successive-SSW frequency forced by present-day or future SIC is larger than that forced by preindustrial SIC.

ARTICLE IN PRESS

CMIP6 models with lower Arctic SIC consistently simulate a higher frequency of SSWs and successive SSWs, effectively ruling out that increasing greenhouse gases alone are responsible for the trend. The robust negative correlation between SIC and SSW frequency across models provides high-confidence evidence that Arctic sea ice loss is the key forcing agent for SSW increases.

Our research provides observational and modeling evidence that increases in successive SSWs—and the associated anomalous cold air outbreaks—is very likely forced by the decline in Arctic sea ice. This suggests that despite global warming, cold anomaly amplitudes on northern continents may not weaken as projected in the future as stratospheric variability is reshaped by a warming Arctic, consistent with other recent studies[51].

Although we compare the SIC state in different CESM2-WACCM experiments versus that in CMIP6 multimodel historical runs, it is not easy to separate the role of Arctic SIC loss from external forcing. The PAMIP experiments more directly confirm the role of Arctic SIC loss in SSW changes. The pattern scaling technique[52] might be beneficial for comparisons across CMIP6 models in the future study to better understand the potential response of SSWs due to a unit change in SIC loss per Kelvin degree of global warming.

This study tries to understand the relation between SIC and SSW from a linear perspective. Their relation might be nonlinear, and this nonlinearity is likely to amplify under a warming climate. As a potential consequence, the cold anomaly amplitudes following the SSWs seem to saturate in a higher warming scenario: The cold anomalies are larger in some scenarios and smaller in others relative to the historical runs (Figure 6). Further, the SSWs are influenced by different forcings such as ENSO, QBO, and solar cycle. This study also examines the SSWs from PAMIP experiments, which minimize the possible interference from other forcings. The nonlinear impacts of those forcings on SSWs are still not well understood, which deserve deeper investigation in the future.

Methods

Reanalysis and SIC

To give an overview of the increase in SSW frequency and multi-SSW winters, the fifth-

ARTICLE IN PRESS

generation reanalysis from the ECMWF (ERA5) is used in this study[53]. The ERA5 reanalysis provides an identical horizontal resolution for latitude and longitude (0.25° × 0.25°) at 137 model levels. For this study, the data are collected at 1°×1° horizontal resolution and 37 standard pressure levels for easy handling and storage. Variables collected include the air temperature, geopotential height, zonal wind (u-wind), and meridional wind (v-wind). Daily data are used to calculate the wave activity flux, while the monthly data are used to extract the wave refractive index. The sea ice concentration from the UK Met Office Hadley Center Sea Ice and Sea Surface Temperature dataset (HadISST) is used to examine the SIC state change. This SIC dataset has a as a horizontal resolution of 1° × 1° (latitude × longitude) and spans from 1870 to the present[54].

CESM2-WACCM and experiments

CESM1-WACCM has been recognized as one of the top-performing CMIP5 models in stratospheric simulation[55]. CESM2-WACCM, developed by the National Center for Atmospheric Research (NCAR), builds on this CESM1-WACCM foundation with upgrades such as refined atmospheric physics parameterizations, enhanced capabilities for representing the middle and upper atmosphere, and improvements in chemical modules. CESM2-WACCM utilizes WACCM6 as its atmospheric component[56]. WACCM6 has 70 sigma/pressure levels ranging from 1000 hPa to 4.5×10^{-6} hPa, and a horizontal resolution of 0.9° (latitude) × 1.25° (longitude). This represents an enhancement over the earlier CESM1-WACCM. By default, WACCM6 operates at a horizontal resolution four times that of WACCM4, leading to better representation of stratospheric variability—including a self-generated quasi-biennial oscillation (QBO) and a more accurate climatology of sudden stratospheric warmings (SSWs)[49,57]. Additionally, the updated orographic gravity wave scheme now considers blocking effects from topographic ridges.

CESM2-WACCM is a comprehensive Earth system model featuring coupled interactions among the atmosphere, land, ocean, rivers, sea ice, land ice, and ocean waves. As one of the CMIP6 models, CESM2-WACCM is capable of simulating different aspects of the stratospheric circulation[57,58], and the atmospheric teleconnections associated with the Arctic SIC are also resolved by this model[59]. CESM2-WACCM contributes to the Coupled Model Intercomparison

ARTICLE IN PRESS

Project Phase 6 (CMIP6) in different experiment families. The experiment outputs with available SIC and daily u-wind and surface air temperature (tas) are employed in this model. A variety of experiments in different scenarios are available for analyzing the SIC state and the SSW characteristics.

The first simulation family are the DECK (Diagnostic, Evaluation and Characterization of Klima) experiments: Pre-industrial control (piControl), Abrupt quadrupling of CO2 concentration (abrupt-4×CO_2), and 1% yr^{-1} CO_2 concentration increase (1pctCO_2). The piControl run simulates climate under constant pre-industrial forcing conditions without external forcings, with a minimum run time of 500 years[60]. The 1pctCO_2 run branches from the piControl simulation, with global annual mean CO_2 concentration increasing by 1% per year from the 1850 piControl baseline. The simulation runs for at least 150 years[60]. The abrupt-4×CO_2 run is based on piControl, instantly quadrupling the 1850 global annual mean CO_2 concentration from piControl and maintaining it, with all other forcings identical to piControl. The simulation also runs for at least 150 years[60].

The second simulation family are the historical runs. This simulation is also branched from piControl. The historical experiment evaluates the model's capability to simulate climate change and analyze its response to observed external forcings such as volcanic aerosols, solar variability, and varying atmospheric composition (GHGs and aerosols) due to human activities. It covers the period from 1850 to 2014[60].

The third simulation family are the experiments for the Scenario Model Intercomparison Project (ScenarioMIP). In the Shared Socioeconomic Pathways (ssp) scenarios, each SSP represents a distinct socio-economic development pathway[61]. Specifically, SSP126 depicts a sustainable pathway with low radiative forcing, characterized by low vulnerability and mitigation challenges. SSP245 represents an intermediate pathway with moderate radiative forcing, reflecting moderate social vulnerability and relatively mild land use and aerosol changes. SSP370 corresponds to a regional rivalry scenario, marked by moderate economic growth, rapid population increase, slow energy sector transformation, and high unmitigated emissions, making mitigation difficult. SSP370-lowNTCF is similar to SSP370 but with low NTCF emissions. SSP585

ARTICLE IN PRESS

represents a high-energy consumption socioeconomic pathway combined with a strong radiative forcing scenario, reaching a peak radiative forcing of 8.5 W m^{-2} by 2100. SSP534-over is overshoot of 3.4 W/m^2 branching from SSP585 in 2040. The available ScenarioMIP experiments with SIC outputs from CESM2-WACCM include SSP126, SSP245, SSP370, SSP534-over, and SSP585, which provide different Arctic SIC state under a series of socioeconomic pathways.

The abundant experiments by CESM2-WACCM provide large SSW samples (and multi-SSW winters) and build a robust statistical relationship between the Arctic SIC and SSWs.

Sensitivity experiments

To examine the possible driving of the SSW frequency change by the mean Arctic SIC state, a control experiment is performed using CESM2-WACCM. In the control experiment, the global SST and SIC are fixed at the 1979-1999 mean climatological level, with the other forcings set at the 2000 level. This experiment is aimed to examine the mean SSW frequency and the frequency of multi-SSW winters. In the sensitivity experiment, the global SST (including the Arctic Ocean with sea ice lost) is still fixed at the 1979-1999 climatological state, while the Arctic SIC is changed to the 2000-2024 climatological level. The sensitivity experiment aims to isolate the role of SIC for the increased frequency of SSWs and successive SSWs in recent two decades. The control and sensitivity experiments are named SSTp1-SICp1 and SSTp1-SICp2, respectively (p1: 1979-1999; p2: 2000-2024). The two experiments are integrated continuously for 60 years, and the difference between the two experiments is primarily attributed to the SIC forcing change (decline).

CMIP6 models

A series of CMIP6 experiments, coordinated by the Working Group on Coupled Modelling (WGCM) under the World Climate Research Programme (WCRP), were designed to provide climate model outputs for the Intergovernmental Panel on Climate Change (IPCC) reports (e.g., AR6). With this long integration in the historical runs, more successive SSWs (and therefore multi-SSW winters) can be identified. To examine the relationship between SIC and the SSWs among models, the historical runs with a timespan of 1850-2014 are used. Models with available daily u-wind, daily tas, and monthly SIC are used. Finally, 34 CMIP6 models are selected to study the

ARTICLE IN PRESS

relationship between the mean Arctic SIC state and mean SSW frequency. The details of the 34 models used in the study are shown in Supplementary Table 1, where the affiliation, horizontal resolution, vertical layers, and the atmospheric model top are listed. The statistics of the SSWs from different datasets are shown in Supplementary Table 2.

PAMIP experiments

Considering that atmospheric internal variability is large but the SIC signals are small and difficult to detect, model experiments with a large sample size that isolate the role of SIC[62,63] are needed to robustly construct the relation between Arctic SIC and SSWs[62,64]. The Polar Amplification Model Intercomparison Project (PAMIP) experiments provide the climate response to a series of SIC state forcings. As shown in Supplementary Table 3, the No. 1 experimental group (pdSST-pdSIC) uses a global atmospheric model to simulate the present-day climate, constrained by present-day estimates of sea surface temperature (SST) and sea ice concentration (SIC). The present-day SST (pdSST) and SIC (pdSIC) are the 1979–2000 climatology derived from the HadISST. The No. 2 experimental group (pdSST-piArcSIC) uses pre-industrial Arctic SIC (piArcSIC) as the forcing. Pre-industrial Arctic SIC (piArcSIC) is derived from a 31-member ensemble of historical CMIP5 model outputs, with the 1979–2000 warming signal removed. The No. 3 experimental group is the same as the No. 1 experimental group (pdSST-pdSIC), except that the Arctic SIC is replaced by the future Arctic SIC (futArcSIC). The future Arctic SIC (futArcSIC) is derived from an ensemble of 31 CMIP5 RCP8.5 simulations, representing a 2°C warming scenario. The PAMIP experiments are integrated for 14 months, starting on 1 April 2000. Each experiment comprises at least 100 ensemble members, with identical forcing conditions for SST and SIC. Four models with all of the three experiments available are employed, including AWI-CM-1-1-MR, CanESM5, HadGEM3-GC31-MM, and IPSL-CM6A-LR. Two of them suffer from a poor simulation of SSWs, and so we focus only on two of the models.

Algorithms: SSW identification and determination of successive SSWs

Following the World Meteorological Organization (WMO) definition, an SSW event is

ARTICLE IN PRESS

identified when the zonal-mean u-wind at 60°N/10 hPa reverse to easterlies and the temperature gradient from 60° N to 90° N also reverses[65,66]. Considering that some marginal SSWs show the wind reversal farther poleward in observations, the zonal-mean u-wind at 65°N and 70°N is also examined to identify those events[59]. Once an SSW is identified, no new ones occur within the following 20 days when consecutive westerlies follow considering that the u-wind still frequently fluctuates during some SSW cases.

In this study, the successive SSWs within a winter are also counted, and those winters with more than one SSW are termed multi-SSW winters. The multi-SSW winters occur much less frequently than the single-SSW winters and non-SSW winters. This study reveals that the multi-SSW winter frequency increases in a less Arctic SIC world, which is shown to be associated with changes of the meridional gradient of potential vorticity and therefore the refractive index due to Arctic SIC decline[44,46]. In our algorithm, we optimize the SSW identification method by examining the time of two neighboring numbered SSWs. If their time difference is less than 3 months, which indicated both of them occur in the same winter, the second SSW is a successive one and its attribute No. increases by 1. Otherwise, all SSWs in single-SSW winters is given the attribute No. 1. In this manner, the attribute No. of the identified SSWs has a minimum value of 1, and increases by 1 if the former event is also in the same winter.

If a third SSW happens in a given winter, then this winter is assigned attribute No. = 3. After examining the SSWs from different datasets, including CESM2-WACCM experiments, historical simulations in CMIP6 models, and sensitivity runs, we never find a winter with four or more SSWs. All SSWs are finally distributed under the attribute No. The total number of winters with two or more SSWs is the number of multi-SSW winters.

Dynamic analysis tools and statistical methods

The quasi-geostrophic refractive index provides a diagnostic of the effect of planetary wave propagation by the background zonal flow[67,68] and is expressed as:

$$n^2 = \underbrace{\frac{\bar{q}_\varphi}{a\bar{u}}}_{\text{Term A}} - \underbrace{\frac{s^2}{a^2\cos^2\varphi}}_{\text{Term B}} - \underbrace{\frac{f^2}{4N^2H^2}}_{\text{Term C}}, \quad (1)$$

ARTICLE IN PRESS

where overbars and subscripts denote zonal means and derivatives, respectively. Decrease in SIC modifies the static stability and weakens N^2, and changes in N^2 can well explain term C, since term C $\propto -1/N^2$, and (termC)′ $\propto -(1/N^2)' = (N^2)'/(N^2)^2 \propto (N^2)'$, where the prime indicates a small deviation from a reference value (i.e., the ensemble means shown in the red dots in Figure 7). In particular, the meridional gradient of the zonal-mean potential vorticity, $\bar{q}_\phi$, is given by Andrews et al.[69]:

$$\bar{q}_\varphi = \underbrace{2\Omega\cos\varphi}_{q1} - \underbrace{\frac{\partial}{\partial\varphi}\frac{\frac{\partial}{\partial\varphi}(\bar{u}\cos\varphi)}{a\cos\varphi}}_{q2} - \underbrace{\frac{af^2}{\rho_0}\frac{\partial}{\partial z}\left(\frac{\rho_0}{N^2}\frac{\partial\bar{u}}{\partial z}\right)}_{q3}. \quad (2)$$

Here, Ω and a are Earth's rotation rate and radius; φ, z, s, N and u denote latitude, log-pressure height, zonal wavenumber, buoyancy frequency and zonal winds, respectively; H=7000m is the scale height. The Coriolis parameter is $f = 2\Omega\sin\varphi$, and the reference air density is $\rho_0 = \rho_s \exp(-z/H), \rho_s = 1.2$ kg m^{-3}. A positive value of the refractive index (n^2) indicates regions that support meridional and vertical planetary-wave propagation, while negative values denote evanescent zones or critical layers where propagation is inhibited or wave absorption occurs[64,70]. Larger values correspond to more favorable propagation conditions.

To further examine the source and propagation of wave activity, we compute the Eliassen–Palm (EP) flux, a vector quantity (**F**) that quantifies these meridional and vertical transport of wave activity, as defined by[69]:

$$F_\varphi = \rho_0 a\cos\varphi\left(\frac{\overline{v'\theta'}}{\bar{\theta}_z}\bar{u}_z - \overline{v'u'}\right), \quad (3)$$

$$F_z = \rho_0 a\cos\varphi\left(\frac{\overline{v'\theta'}}{\bar{\theta}_z}\left(f - \frac{1}{a\cos\varphi}(\bar{u}\cos\varphi)_\varphi\right) - \overline{w'u'}\right). \quad (4)$$

The divergence of the EP flux (EPFD), which serves as a diagnostic of wave – mean-flow interactions, is formulated as[71]:

$$\nabla\cdot\boldsymbol{F} = \left[\frac{1}{a\cos\varphi}\frac{\partial}{\partial\varphi}\left(F_\varphi\cos\varphi\right) + \frac{\partial F_z}{\partial z}\right], \quad (5)$$

where v, w and θ represent the meridional wind, vertical wind, and potential temperature,

ARTICLE IN PRESS

respectively. Primes denote deviations from the zonal mean, while other parameters follow the definitions above. A positive (negative) EPFD indicates a source (sink) of wave activity, corresponding to momentum deposition that accelerates (decelerates) the mean flow[72].

Finally, the robustness of the diagnosed relationships is evaluated using Pearson correlation coefficients. The statistical significance of correlation and composite analyses is tested with the t-test. The frequency difference between two samples is tested with the bootstrapping method.

Data availability

The outputs of CMIP6 and PAMIP are available at https://esgf-node.llnl.gov/projects/esgf-llnl/. Other dataset resource shows below: ERA5 is obtained from https://cds.climate.copernicus.eu/. Sea ice data can be download at https://www.metoffice.gov.uk/hadobs/hadisst2/data/download.html.

Code availability

The CESM2 model code is freely available from https://github.com/ESCOMP/CESM. The codes for creating the figures and analyses were written in NCAR Command Language Version 6.4. The source codes for the analysis of this study are available from https://figshare.com/s/42afcbefed2a4dd84323?file=58489087.

ARTICLE IN PRESS

References

1. Yadav, J., Kumar, A. & Mohan, R. Dramatic decline of Arctic sea ice linked to global warming. *Natural Hazards*. **103**, 2617-2621 (2020).

2. Kwok, R. & Rothrock, D. A. Decline in Arctic sea ice thickness from submarine and ICESat records: 1958–2008. *Geophysical Research Letters*. **36** (2009).

3. Cavalieri, D. J. & Parkinson, C. L. Arctic sea ice variability and trends, 1979-2010. *Cryosphere*. **6**, 881-889 (2012).

4. Stroeve, J. C., Markus, T., Boisvert, L., Miller, J. & Barrett, A. Changes in Arctic melt season and implications for sea ice loss. *Geophysical Research Letters*. **41**, 1216-1225 (2014).

ARTICLE IN PRESS

5. Boé, J., Hall, A. & Qu, X. September sea-ice cover in the Arctic Ocean projected to vanish by 2100. *Nature Geoscience*. **2**, 341-343 (2009).

6. Notz, D. & Marotzke, J. Observations reveal external driver for Arctic sea-ice retreat. *Geophysical Research Letters*. **39** (2012).

7. Ding, Q. et al. Influence of high-latitude atmospheric circulation changes on summertime Arctic sea ice. *Nature Climate Change*. **7**, 289-295 (2017).

8. Stroeve, J. C. et al. The Arctic's rapidly shrinking sea ice cover: a research synthesis. *Climatic Change*. **110**, 1005-1027 (2012).

9. Min, S.-K., Zhang, X., Zwiers, F. W. & Agnew, T. Human influence on Arctic sea ice detectable from early 1990s onwards. *Geophysical Research Letters*. **35** (2008).

10. Stroeve, J. & Notz, D. Changing state of Arctic sea ice across all seasons. *Environmental Research Letters*. **13**, 103001 (2018).

11. Notz, D. & Stroeve, J. Observed Arctic sea-ice loss directly follows anthropogenic CO2 emission. *Science*. **354**, 747-750 (2016).

12. Deser, C., Walsh, J. E. & Timlin, M. S. Arctic sea ice variability in the context of recent atmospheric circulation trends. *Journal of Climate*. **13**, 617-633 (2000).

13. Hu, A., Rooth, C., Bleck, R. & Deser, C. NAO influence on sea ice extent in the Eurasian coastal region. *Geophysical Research Letters*. **29**, 2053 (2002).

14. Ogi, M., Yamazaki, K. & Wallace, J. M. Influence of winter and summer surface wind anomalies on summer Arctic sea ice extent. *Geophysical Research Letters*. **37**, 07701 (2010).

15. Mahajan, S., Zhang, R. & Delworth, T. L. Impact of the Atlantic meridional overturning circulation (AMOC) on Arctic surface air temperature and sea ice variability. *Journal of Climate*. **24**, 6573-6581 (2011).

16. Day, J. J., Hargreaves, J. C., Annan, J. D. & Abe-Ouchi, A. Sources of multi-decadal variability in Arctic sea ice extent. *Environmental Research Letters*. **7**, 034011 (2012).

17. Petoukhov, V., Rahmstorf, S., Petri, S. & Schellnhuber, H. J. Quasiresonant amplification of planetary waves and recent Northern Hemisphere weather extremes. *Proceedings of the*

ARTICLE IN PRESS

ARTICLE IN PRESS

National Academy of Sciences. **110**, 5336-5341 (2013).

18. Screen, J. A. & Simmonds, I. Amplified mid-latitude planetary waves favour particular regional weather extremes. *Nature Climate Change*. **4**, 704-709 (2014).
19. Kim, B.-M. et al. Weakening of the stratospheric polar vortex by Arctic sea-ice loss. *Nature Communications*. **5**, 4646 (2014).
20. Zhang, X. et al. The role of Arctic sea ice loss in the interdecadal trends of the East Asian summer monsoon in a warming climate. *npj Climate and Atmospheric Science*. **7**, 174 (2024).
21. Screen, J. A. & Simmonds, I. The central role of diminishing sea ice in recent Arctic temperature amplification. *Nature*. **464**, 1334-1337 (2010).
22. Serreze, M. C., Barrett, A. P. & Stroeve, J. Recent changes in tropospheric water vapor over the Arctic as assessed from radiosondes and atmospheric reanalyses. *Journal of Geophysical Research: Atmospheres*. **117** (2012).
23. Jun, S.-Y., Ho, C.-H., Jeong, J.-H., Choi, Y.-S. & Kim, B.-M. Recent changes in winter Arctic clouds and their relationships with sea ice and atmospheric conditions. *Tellus A: Dynamic Meteorology and Oceanography*. **68**, 29130 (2016).
24. Francis, J. A., Chan, W., Leathers, D. J., Miller, J. R. & Veron, D. E. Winter Northern Hemisphere weather patterns remember summer Arctic sea-ice extent. *Geophysical Research Letters*. **36** (2009).
25. Liu, J., Curry, J. A., Wang, H., Song, M. & Horton, R. M. Impact of declining Arctic sea ice on winter snowfall. *Proceedings of the National Academy of Sciences*. **109**, 4074-4079 (2012).
26. Francis, J. A. & Vavrus, S. J. Evidence for a wavier jet stream in response to rapid Arctic warming. *Environmental Research Letters*. **10**, 014005 (2015).
27. Luo, D. et al. Impact of Ural blocking on winter warm Arctic-cold Eurasian anomalies. Part I: Blocking-induced amplification. *Journal of Climate*. **29**, 3925-3947 (2016).
28. Sun, L., Deser, C. & Tomas, R. A. Mechanisms of stratospheric and tropospheric circulation response to projected Arctic sea ice loss. *Journal of Climate*. **28**, 7824-7845 (2015).
29. Baldwin, M. P. & Dunkerton, T. J. Stratospheric harbingers of anomalous weather regimes.

ARTICLE IN PRESS

Science. **294**, 581-584 (2001).

30. Baldwin, M. P. et al. Sudden stratospheric warmings. *Reviews of Geophysics*. **59**, e2020RG000708 (2021).
31. Rao, J. et al. Predictability of stratospheric sudden warmings in the Beijing Climate Center forecast system with statistical error corrections. *Journal of Geophysical Research: Atmospheres*. **124**, 8385-8400 (2019).
32. Reichler, T., Kim, J., Manzini, E. & Kröger, J. A stratospheric connection to Atlantic climate variability. *Nature Geoscience*. **5**, 783-787 (2012).
33. Baldwin, M. P. & Holton, J. R. Climatology of the stratospheric polar vortex and planetary wave breaking. *Journal of Atmospheric Sciences*. **45**, 1123-1142 (1988).
34. Pogoreltsev, A. I. et al. Interannual and intraseasonal variability of stratospheric dynamics and stratosphere–troposphere coupling during northern winter. *Journal of Atmospheric and Solar-Terrestrial Physics*. **136**, 187-200 (2015).
35. Song, K. & Son, S.-W. Revisiting the ENSO–SSW relationship. *Journal of Climate*. **31**, 2133-2143 (2018).
36. Richter, J. H., Matthes, K., Calvo, N. & Gray, L. J. Influence of the quasi-biennial oscillation and El Niño–Southern Oscillation on the frequency of sudden stratospheric warmings. *Journal of Geophysical Research: Atmospheres*. **116,** D20111 (2011).
37. Butler, A. H. & Polvani, L. M. El Niño, La Niña, and stratospheric sudden warmings: A reevaluation in light of the observational record. *Geophysical Research Letters*. **38**, L13807 (2011).
38. Li, Y. et al. The connection between the second leading mode of the winter North Pacific sea surface temperature anomalies and stratospheric sudden warming events. *Climate Dynamics*. **51**, 581-595 (2018).
39. Zhang, J., Orsolini, Y. J., Limpasuvan, V. & Ukita, J. Impact of the Pacific sector sea ice loss on the sudden stratospheric warming characteristics. *npj Climate and Atmospheric Science*.

ARTICLE IN PRESS

ARTICLE IN PRESS

5, 74 (2022).

40. Zhang, P., Wu, Y. & Smith, K. L. Prolonged effect of the stratospheric pathway in linking Barents–Kara Sea sea ice variability to the midlatitude circulation in a simplified model. *Climate Dynamics*. **50**, 527-539 (2018).
41. King, M. P., Hell, M. & Keenlyside, N. Investigation of the atmospheric mechanisms related to the autumn sea ice and winter circulation link in the Northern Hemisphere. *Climate Dynamics*. **46**, 1185-1195 (2016).
42. Hoshi, K. et al. Weak stratospheric polar vortex events modulated by the Arctic sea-ice loss. *Journal of Geophysical Research: Atmospheres*. **124**, 858-869 (2019).
43. Ineson, S. et al. Statistics of sudden stratospheric warmings using a large model ensemble. *Atmospheric Science Letters*. **25**, e1202 (2023).
44. Lu, Q. et al. Stratosphere-troposphere coupling during stratospheric extremes in the 2022/23 winter. *Weather and Climate Extremes*. **42**, 100627 (2023).
45. Lee, S. H., Butler, A. H. & Manney, G. L. Two major sudden stratospheric warmings during winter 2023/2024. *Weather*. **80**, 45-53 (2025).
46. Lu, Q., Rao, J., Ren, R., Shi, C. & Liu, S. Enhanced stratosphere-troposphere and tropics-Arctic couplings in the 2023/24 winter. *Communications Earth & Environment*. **5**, 631 (2024).
47. Cohen, J., Agel, L., Barlow, M. & Entekhabi, D. No detectable trend in mid-latitude cold extremes during the recent period of Arctic amplification. *Communications Earth & Environment*. **4** (2023).
48. Kretschmer, M. et al. More-persistent weak stratospheric polar vortex states linked to cold extremes. *Bulletin of the American Meteorological Society*. **99**, 49-60 (2018).
49. Rao, J. & Garfinkel, C. I. CMIP5/6 models project little change in the statistical characteristics of sudden stratospheric warmings in the 21st century. *Environmental Research Letters*. **16**, 034024 (2021).
50. Blackport, R., Sigmond, M. & Screen, J. A. Models and observations agree on fewer and milder midlatitude cold extremes even over recent decades of rapid Arctic warming. *Science*

ARTICLE IN PRESS

Advances. **10**, eadp1346 (2024).

51. Cohen, J., Agel, L., Barlow, M., Garfinkel, C. I. & White, I. Linking Arctic variability and change with extreme winter weather in the United States. *Science*. **373**, 1116-1121 (2021).
52. Tebaldi, C. & Arblaster, J. M. Pattern scaling: Its strengths and limitations, and an update on the latest model simulations. *Climatic Change*. **122**, 459-471 (2014).
53. Hersbach, H. et al. The ERA5 global reanalysis. *Quarterly Journal of the Royal Meteorological Society*. **146**, 1999-2049 (2020).
54. Rayner, N. A. et al. Global analyses of sea surface temperature, sea ice, and night marine air temperature since the late nineteenth century. *Journal of Geophysical Research: Atmospheres*. **108,** D14, 4407, (2003).
55. Marsh, D. R. et al. Climate Change from 1850 to 2005 simulated in CESM1(WACCM). *Journal of Climate*. **26**, 7372-7391 (2013).
56. Gettelman, A. et al. High climate sensitivity in the community earth system model version 2 (CESM2). *Geophysical Research Letters*. **46**, 8329-8337 (2019).
57. Rao, J., Garfinkel, C. I. & White, I. P. Projected strengthening of the extratropical surface impacts of the stratospheric quasi-biennial oscillation. *Geophysical Research Letters*. **47**, e2020GL089149 (2020).
58. Rao, J. & Garfinkel, C. I. Projected changes of stratospheric final warmings in the Northern and Southern Hemispheres by CMIP5/6 models. *Climate Dynamics*. **56**, 3353-3371 (2021).
59. Chen, H., Rao, J., Yang, H., Luo, J. & Wu, G. Underrepresentation of the linkage between the Barents-Kara sea ice and east Asian rainfall in early summer by CMIP6 models. *Atmosphere*. **14**, 1044 (2023).
60. Eyring, V. et al. Overview of the coupled model intercomparison project phase 6 (CMIP6) experimental design and organization. *Geoscientific Model Development*. **9**, 1937-1958 (2016).
61. O'Neill, B. C. et al. The scenario model intercomparison project (ScenarioMIP) for CMIP6. *Geoscientific Model Development*. **9**, 3461-3482 (2016).

ARTICLE IN PRESS

ARTICLE IN PRESS

62. Sun, L., Deser, C., Simpson, I. & Sigmond, M. Uncertainty in the winter tropospheric response to Arctic Sea ice loss: The role of stratospheric polar vortex internal variability. *Journal of Climate*. **35**, 3109-3130 (2022).

63. Peings, Y., Labe, Z. M. & Magnusdottir, G. Are 100 ensemble members enough to capture the remote atmospheric response to +2°C Arctic sea ice loss? *Journal of Climate*. **34**, 3751-3769 (2021).

64. Smith, D. M. et al. Robust but weak winter atmospheric circulation response to future Arctic sea ice loss. *Nature Communications*. **13**, 727 (2022).

65. Charlton, A. J. & Polvani, L. M. A new look at stratospheric sudden warmings. Part I: Climatology and modeling benchmarks. *Journal of Climate*. **20**, 449-469 (2007).

66. Butler, A. H. et al. Defining sudden stratospheric warmings. *Bulletin of the American Meteorological Society*. **96**, 1913-1928 (2015).

67. Chen, P. & Robinson, W. A. Propagation of planetary waves between the troposphere and stratosphere. *Journal of Atmospheric Sciences*. **49**, 2533-2545 (1992).

68. Weinberger, I., Garfinkel, C. I., White, I. P. & Birner, T. The efficiency of upward wave propagation near the tropopause: Importance of the form of the refractive index. *Journal of the Atmospheric Sciences*. **78**, 2605-2617 (2021).

69. Andrews, D. G., Leovy, C. B. & Holton, J. R. *Middle atmosphere dynamics*. Vol. 40 (Academic press, 1987).

70. Matsuno, T. Vertical propagation of stationary planetary waves in the winter northern hemisphere. *Journal of Atmospheric Sciences*. **27**, 871-883 (1970).

71. Jucker, M. Scaling of Eliassen-Palm flux vectors. *Atmospheric Science Letters*. **22**, e1020 (2021).

72. Yasui, R., Sato, K. & Miyoshi, Y. Roles of Rossby waves, Rossby-gravity waves, and gravity waves generated in the middle atmosphere for interhemispheric coupling. *Journal of the Atmospheric Sciences*. **78**, 3867-3888 (2021).

ARTICLE IN PRESS

ARTICLE IN PRESS

Acknowledgments

We thank all data providers: UK Met Office, ESGF and ECMWF. We also acknowledge the National Natural Science Foundation of China, the Israel Science Foundation, the National Science Foundation, and the Qinglan Project of Jiangsu of China for the fundings.

Funds

This work was supported by the National Natural Science Foundation of China (grant Nos. 42322503, 42361144843, and 42505036), the Israel Science Foundation (grant no. 3065/23), and the Qinglan Project of Jiangsu of China. J.C. is supported by the National Science Foundation grant AGS-2140909.

Competing interests

The authors have no competing interests to declare that are relevant to the content of this article.

Author Contributions

Methodology: Jian Rao. Investigation: Jian Rao. Visualization: Jian Rao. Supervision: Chaim I. Garfinkel, Judah Cohen. Writing—original draft: Jian Rao. Writing—review & editing: Chaim I. Garfinkel, Judah Cohen, Yue Wang, Xiaoqi Zhang, Rongcai Ren, and Pengfei Zhang.

ARTICLE IN PRESS

ARTICLE IN PRESS

Editorial summary:
New evidence shows successive sudden stratospheric warmings have been increasing, with broader cold air influence in the northern hemisphere continents. Multimodel historical simulations and polar climate modeling attribute this change to the Arctic sea ice decline.

Peer review information:
Communications Earth and Environment thanks Yannick Peings, Ryan Williams and the other, anonymous, reviewer(s) for their contribution to the peer review of this work. Primary Handling Editors: Seung-Ki Min, Alireza Bahadori and Alice Drinkwater. A peer review file is available.

ARTICLE IN PRESS